Evidence for Truncated Exponential Probability Distribution of Earthquake Slip

Article *in* Bulletin of the Seismological Society of America · July 2016

DOI: 10.1785/0120150291

CITATIONS
46

READS
786

2 authors:

Kiran Kumar Thingbaijam
GNS Science
44 PUBLICATIONS **2,499** CITATIONS
SEE PROFILE

P. M. Mai
King Abdullah University of Science and Technology
267 PUBLICATIONS **8,800** CITATIONS
SEE PROFILE

Bulletin of the Seismological Society of America, Vol. 106, No. 4, pp. 1802–1816, August 2016, doi: 10.1785/0120150291

Ⓔ

Evidence for Truncated Exponential Probability Distribution of Earthquake Slip

by Kiran K. S. Thingbaijam and P. Martin Mai

Abstract Earthquake ruptures comprise spatially varying slip on the fault surface, where slip represents the displacement discontinuity between the two sides of the rupture plane. In this study, we analyze the probability distribution of coseismic slip, which provides important information to better understand earthquake source physics. Although the probability distribution of slip is crucial for generating realistic rupture scenarios for simulation-based seismic and tsunami-hazard analysis, the statistical properties of earthquake slip have received limited attention so far. Here, we use the online database of earthquake source models (SRCMOD) to show that the probability distribution of slip follows the truncated exponential law. This law agrees with rupture-specific physical constraints limiting the maximum possible slip on the fault, similar to physical constraints on maximum earthquake magnitudes. We show the parameters of the best-fitting truncated exponential distribution scale with average coseismic slip. This scaling property reflects the control of the underlying stress distribution and fault strength on the rupture dimensions, which determines the average slip. Thus, the scale-dependent behavior of slip heterogeneity is captured by the probability distribution of slip. We conclude that the truncated exponential law accurately quantifies coseismic slip distribution and therefore allows for more realistic modeling of rupture scenarios.

Online Material: Figures showing scaling of slip area with seismic moment and Q–Q plots and tables listing earthquakes, rupture models, and fits of various distributions to the empirical probability distribution.

Introduction

Earthquakes are governed by space–time-dependent multiscale processes in the rock volume, including the stress state on the rupture plane just prior to nucleation, the strength of the host rock, as well as frictional properties along the contact surface. The resulting coseismic slip and its statistical properties record the effects of the underlying nonlinear dynamic processes. Knowledge of the statistical properties of the slip not only sheds light on earthquake dynamics but also allows seismologists to generate realistic rupture scenarios for physics-based ground-motion simulations (Somerville *et al.*, 1999; Mai and Beroza, 2002; Guatteri *et al.*, 2004; Lavallée *et al.*, 2006; Liu *et al.*, 2006; Gusev, 2011; Mena *et al.*, 2012; Song *et al.*, 2013; Goda *et al.*, 2014). In case of shaking simulations using a kinematic characterization of the earthquake rupture process, which includes the slip, the local on-fault slip functions are convolved with appropriate Green's functions to compute the resulting ground shaking. Consequently, the statistical properties of slip strongly govern the simulated ground motions (e.g., Song and Dalguer, 2013). The probability distribution of slip (or frequency-slip distribution) determines the proportions of slip asperities (i.e., patches of large slip on the fault) that contribute to the radiated seismic wavefield. However, this statistical property of slip and its characteristics remain elusive so far, mostly due to the limited available data on earthquake slip measurements.

Previous attempts to characterize the probability distribution of slip produced ambiguous findings. Lavallée *et al.* (2006) suggested that a non-Gaussian Lévy law reproduces the spatial variability of slip implied by the frequency-slip distribution. Their conclusion is based on analyzing rupture models for four earthquakes. In contrast, Gusev (2011) postulated that the probability distribution of slip follows a modified-lognormal distribution. Investigating 37 selected rupture models, he observed that the empirical distributions do not support the hypothesis of non-Gaussian Lévy law for slip heterogeneity. However, because each of these studies used a very limited dataset of earthquake slip measurements, their results may only be applicable for the particular datasets. The goal of our study is a more objective assessment based on a large database of earthquake-rupture models to

better elucidate the probability distribution of slip and its characteristics and to also link the probability distribution of slip to the underlying rupture physics.

In recent years, inversions of seismic and/or geodetic data are almost routinely carried out to map the spatiotemporal properties of earthquake source kinematics. At the same time, studies based on dynamic rupture (forward) modeling investigate earthquake source complexity from fundamental principles of stress and friction acting in a prestressed heterogeneous Earth (e.g., Day, 1982; Madariaga *et al.*, 1998; Shi and Day, 2013). However, the stress conditions and frictional parameters acting on the fault plane prior to an earthquake are currently not well known. Additionally, not only kilometer-scale fault geometry (e.g., Oglesby *et al.*, 2008; Oglesby and Mai, 2012) but also meter-scale rupture-plane roughness (e.g., Dunham *et al.*, 2011; Fang and Dunham, 2013; Zielke and Mai, 2016) strongly influence the rupture processes, and with that influence the resulting slip pattern and seismic radiation. Source inversions that image the kinematics of the highly nonlinear dynamic rupture process on a complex fault system provide a simplified and bandlimited representation of the rupture evolution in space and time. Nevertheless, the information about slip on the fault contained in such rupture models is still the most reliable measure of the coseismic fault displacement resulting from the dynamic earthquake rupture process. Consequently, the inferred characteristics of slip sparked further research on earthquake-source complexity. For example, the inferred rupture models helped to interpret the underlying dynamic parameters (Tinti *et al.*, 2005; Mai *et al.*, 2006; Causse *et al.*, 2013), to detect self-healing slip pulses (Heaton, 1990), to establish the fractal nature of the slip heterogeneity (Mai and Beroza, 2002), and to develop earthquake-scaling relationships (Somerville *et al.*, 1999; Mai and Beroza, 2000; Strasser *et al.*, 2010).

In this study, we investigate the probability distribution of earthquake slip using the SRCMOD database (Mai and Thingbaijam, 2014). This database currently comprises more than 300 rupture models for earthquakes that occurred globally during the last three decades. We organize this article into two major sections. In the first part, we describe the data selection, data processing, and the methods adopted for the analysis. For the data analysis, we consider two approaches: first, the overall shape of the probability distribution (or average distribution considering ensemble of models) and second, the probability distribution of slip for individual rupture models. In both cases, we analyze how well different statistical distributions characterize the empirical distributions. In the second part, we present the results and discuss their implications in the context of slip heterogeneity and generating scenario earthquake ruptures. Our analyses reveal that a truncated exponential law governs the probability distribution of earthquake slip, consistent with physical constraints on the possible maximum slip. It follows that spatially variable prestress conditions on fault systems characterized by highly localized zones of large stress dominate the space–time evolution of the coseismic rupture process.

Data and Methods

Data Selection

The present study is based on a global database of published earthquake rupture models (see Data and Resources). To ensure statistical significance of the analysis, we exclude coarsely parameterized rupture models with less than 50 spatial data points (subfaults), with less than 15 unique slip values, and those with nonuniform spatial sampling. We also remove smaller events (magnitude $M_w < 5.0$) that are likely to be less well resolved in the inversions. Because seismological instrumentation prior to 1970 was very limited, we also exclude events that occurred before 1970. Finally, in case the same author(s) published multiple rupture models for the same event, we use their latest version and exclude prior ones. Thus, our analysis uses 190 rupture models (Ⓔ Table S1, available in the electronic supplement to this article).

These rupture models were inferred applying a variety of inversion techniques that use different types of data. Therefore, any potential bias in the analysis due to methodological or data-related effects is minimized. However, different source-inversion approaches add to the variability in rupture models for the same event, illustrating the nonuniqueness of finite-fault earthquake-source inversions (e.g., Mai *et al.*, 2016). To assess the potential influence of source-inversion approaches, we separately analyze different subsets of the database extracted using the following criteria: (1) excluding fast finite-fault models, (2) excluding fast finite-fault models and models derived using only geodetic data, (3) considering only results from joint inversions (i.e., multiple types of data use for the inversions), and (4) considering only results from joint inversions but excluding those with minimum slip greater than zero. Fast finite-fault models refer to those generated in a semiautomated fashion within hours of a sizeable earthquake. These models are expected to have larger uncertainties. The second criteria accounts for the limited depth resolution of geodetic data to image slip on the fault. The last criterion rejects those models that might have been reconstructed to compensate deficits of seismic moment (Gusev, 2011).

Data Processing

The source-inversion procedure may result in superfluous low slip at the fault edges of a rupture models, because the assumed rupture dimensions prior to the actual inversions may be chosen too large. Therefore, we trim the rupture models to their effective source dimensions (Somerville *et al.*, 1999; Mai and Beroza, 2000), using a trimming procedure that extends the approach of Mai and Beroza (2000). We estimate effective fault length and width from the corresponding autocorrelation widths W_{AC}, calculated in along-strike and down-dip direction of the slip distribution. W_{AC} is computed as the area under the autocorrelation function (ACF) of

1D slip function $f * f$ normalized by the zero lag value (Bracewell, 1986).

$$W_{\mathrm{AC}} = \frac{\int_{-\infty}^{\infty}(f * f)dx}{f * f|_{\mathrm{x}=0}}. \quad (1)$$

We construct the slip function f along strike (down dip) by summing up the slip in columns (rows) on the rectangular rupture plane. Using an iterative process, we determine the largest dimension that fits the autocorrelation width, so that the difference between the two is less than or equal to the subfault size. This calculation is done by removing any row (or column) at the fault edge from the model if maximum slip in this row (or column) is less than or equal to a threshold value (initially assigned 0.01 and iteratively incremented by 0.001). At the same time, we apply the following conditions:

1. If large-slip asperity areas are affected, the trimming is reduced so that the resulting dimension encompasses the slip asperity. Following Mai *et al.* (2005), a large-slip asperity is defined by the fault region(s) in which slip is greater than or equal to 1/3 of the overall maximum slip.
2. If the top of the rupture plane is located at the Earth surface, and a large-slip asperity is encountered within 5 km depth, the top of the rupture plane is not trimmed.
3. If isolated large-slip values are found at any of the fault edges (likely due to artifacts in the source inversion), the particular row or column is eliminated. However, large slip is allowed at the topmost fault edge, in case the earthquake ruptured to the surface, and at intersections of fault segments.

We apply this iterative procedure to the (trimmed) slip model until no further trimming is possible under the above conditions. The trimmed slip distribution is then rescaled to conserve the seismic moment. Figure 1a depicts the results obtained by applying this procedure to an exemplary rupture model. For rupture models with multiple segments, this procedure is applied to each fault segment. For source models with down-dip segmentation (varying dip), we adopt an averaged-dip single-plane geometry to evaluate the effective source dimensions.

Probability Distribution of Slip

We consider two aspects of the probability distribution: first, the average distribution derived from an ensemble of rupture models and, second, the probability distribution of slip given by each individual rupture model. To calculate the average distribution, we bin the slip distribution for each rupture model so that each slip bin is defined according to a fraction of the maximum slip. However, we neither bin nor normalize the slip distribution when analyzing the individual rupture models.

To calculate the probability distribution, we adopt the complementary cumulative distribution function (CCDF) for slip formulated as follows:

$$1 - F(u_i) = A(u > u_i)/A(u \geq 0), \quad (2)$$

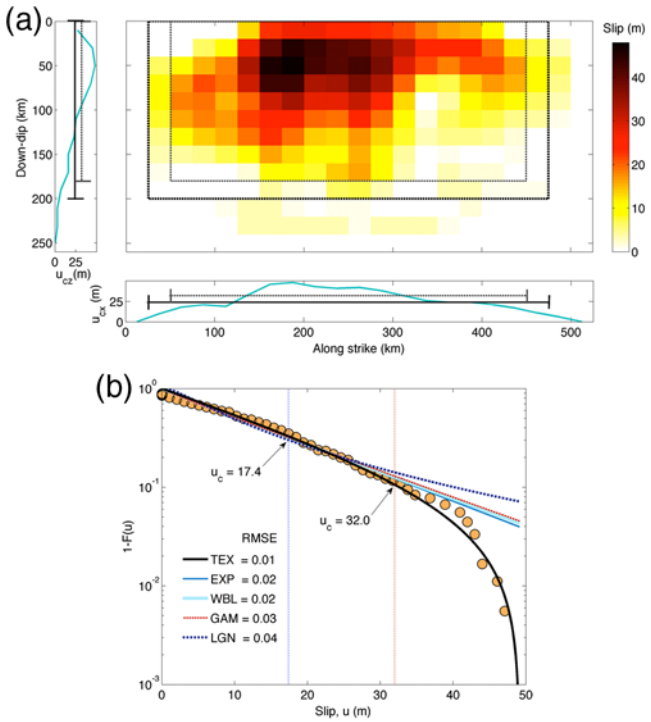

Figure 1. (a) Rupture model for the 2011 Tohoku earthquake (Wei *et al.*, 2012). Effective source dimensions (thick lines) are estimated by adjusting the autocorrelation width of slip summed along dip u_{cz} and strike u_{cx} (lighter lines). (b) Complementary cumulative distribution function (CCDF) of the slip map in (a), with fits of the assumed statistical distributions: truncated exponential (TEX), exponential (EXP), Weibull (WBL), Gamma (GAM), and lognormal (LGN) and their indicated root mean square error (rmse). u_c is the scale parameter of the TEX distribution, and u_t is the largest slip at which the probabilities start deviating from an exponential trend. The color version of this figure is available only in the electronic edition.

in which $A(u > u_i)$ is the integrated area (henceforth called slip area) on the rupture plane that slipped more than a specific value of slip u_i. The CCDF parameterization is similar to the cumulative frequency–magnitude distribution of earthquakes (e.g., Cosentino *et al.*, 1977). The CCDF is also preferred over a histogram-based analysis, because it avoids arbitrary binning of the data, specifically when analyzing individual rupture models. Additionally, the slip-area formulation allows for applying scaling relationships (e.g., seismic moment versus slip area) to calculate average probability distributions.

To compute the average probability distributions, we use ensembles of rupture models for earthquakes classified according to different faulting regimes. Instead of superimposing normalized distributions, we use scaling relationships to better account for different spatial sampling in the rupture-model database and the existence of multiple intraevent models. Although scaling relationships of slip-asperity area versus earthquake magnitude provide an alternative approach for quantifying slip heterogeneity (e.g., Somerville *et al.*, 1999; Mai *et al.*, 2005; Yen and Ma, 2011; Ramírez-Gaytán *et al.*, 2014), we prefer working with probability distributions of slip, because such scaling relationships are relevant

only for the regions of large or very large slip. Also, the concept of slip asperity has not been defined uniformly across these studies. Therefore, we adopt a continuous measure of slip area (i.e., the integrated area on the rupture plane occupied by a specific range of slip) instead of examining a few discrete values of large or very large slip. In this approach, we apply data binning to the slip distributions. Hence, we seek to define an optimal number of bins of slip values that represent the slip distribution. Considering complementary cumulative distribution, the ranges of slip are specified as $u > u_i$, in which u_i is given by the center of each bin. We then develop scaling relationship between the slip areas and seismic moment for the full range of (binned) slip. We also include the total rupture area (i.e., slip area for $u \geq 0$) in our analysis. The scaling relationships are then applied to calculate the average probability distribution.

This binning strategy is aimed at capturing the average probability distribution of the slip distributions effectively. We test different binning techniques to derive the optimal number of bins (Scott, 1979; Freedman and Diaconis, 1981; Shimazaki and Shinomoto, 2007) and also test the square-root rule (i.e., square root of the total number of data points) on each slip model. In all the cases, estimates of optimal bin number cluster between 11 and 14, except for the technique of Shimazaki and Shinomoto (2007) that yields a very large average of 173 bins, with a minimum of 2 and a maximum of 500 bins. Accordingly, we choose the median of 12 bins to partition the range of slip in the rupture models.

We define the scaling relationship of slip area with seismic moment M_0 in a functional form similar to the relation of seismic moment versus rupture area (e.g., Somerville *et al.*, 1999; Mai and Beroza, 2000),

$$\log_{10} A(u > u_i) = \beta_i \log_{10} M_0 + \alpha_i, \tag{3}$$

in which M_0 is seismic moment. To develop the scaling relationships, we apply the orthogonal regression (OR) technique (Fuller, 1987) to account for possible (unknown) errors in both the dependent and independent variable. The OR technique has been used for similar analysis before (e.g., Blaser *et al.*, 2010) and is particularly useful if variables are linearly related with independent and normally distributed errors.

Fits of Different Statistical Distributions

We consider the statistical distributions listed in Table 1 (see also Fig. 1b). The applicability of these statistical distributions is not only justified empirically but is also rooted in the physical context of material failure. The histograms of slip values provided by the rupture models are generally asymmetric and right skewed. Mai *et al.* (2005) suggested that proportions of rupture area occupied by relative slip (i.e., slip area) to the total rupture area follow an exponential distribution. This description corresponds to the CCDF. However, probabilities of very-large-slip values falling short of an exponential decay would yield a truncated exponential distribution. Gusev (2011) suggested that a lognormal distribution captures slip asperities observed in rupture models. The remaining statistical distributions, namely Gamma and Weibull distributions, are widely used to describe failure stress in brittle materials (Basu *et al.*, 2009).

Table 1
The Statistical Distributions Considered in This Study

Distribution	$f(x)$	$1 - F(x)$
Exponential	$h\exp(-hx)$	$\exp(-hx)$
Gamma	$\frac{h}{c}\frac{x^{h-1}}{\Gamma(h)}\exp[-h(x/c)]$	$1 - \frac{\gamma(h,x/c)}{\Gamma(h)}$
Lognormal	$\frac{1}{\sqrt{2h^2\pi}}\frac{1}{x}\exp[-(lnx - c)^2/2h^2]$	$1 - \Phi(\frac{lnx-c}{h})$
Truncated exponential	$\frac{h\exp(-hx)}{1-\exp(-hx_{max})}$	$\frac{\exp(-hx) - \exp(-hx_{max})}{1-\exp(-hx_{max})}$
Weibull	$\frac{h}{c}x^{h-1}\exp[-x^h/c]$	$\exp[-(x/c)^h]$

The scale and shape parameters are denoted by c and h, except for the exponential and truncated exponential distributions, for which h represents the rate parameter. The functions $f(x)$ and $1 - F(x)$ correspond to the probability density function and complementary cumulative distribution function (CCDF) for nonnegative variable x. Γ, γ, and Φ are the Gamma function, the lower incomplete Gamma function, and the cumulative distribution function of the standard normal distribution. x_{max} is the maximum value of the independent variable x.

The slip distributions generally satisfy the (physical) conditions for the Gamma distribution: (1) a finite or fixed number of observations, (2) the expected value of the observations is a positive constant, and (3) a power-law distribution exists for the observations between any given interval (Lienhard and Meyer, 1967). An argument in favor of item (3) would be a power-law probability distribution of slip area or average slip (Kagan, 2005). The physical conditions for a Gamma distribution also hold for the Weibull distribution (Lienhard and Meyer, 1967), used to quantify strength distribution in rocks (e.g., Lobo-Guerrero and Vallejo, 2006; Krumbholz *et al.*, 2014) and to describe earthquake rupture growth (Heimpel, 1996). This distribution assumes a weakest-link hypothesis and is applicable only with power-law distributed (existing) flaws in the material (Bertalan *et al.*, 2014). Earthquake rupture occurs when the tectonic stress exceeds a critical value, corresponding to the strength of the fault (i.e., the material in contact along the rupture surface). Therefore, material properties, stress conditions, and frictional parameters control the amount of coseismic slip. Within this framework of earthquake system science, evaluating slip statistics by testing various statistical distributions and quantifying the best-fitting one provides insight into the physics of earthquake processes.

Goodness-of-Fit Measures

To determine the statistical distribution that best captures the empirical probability distribution of earthquake slip, we compare the fits of the considered statistical distributions. Based on equation 2, we compute the empirical CCDF from the trimmed slip distribution for each rupture model. We then estimate the parameters of the statistical distributions by nonlinear least-squares fitting of the empirical CCDF. Nonlinear least

squares can be applied for all considered statistical distributions and therefore allow for an unbiased comparison of the different statistical distributions (e.g., Krumbholz *et al.*, 2014). For the analysis, we take into account two aspects of the slip distributions. First, we assume that low-slip values are associated with larger uncertainties. This can be explained by the fact that low-slip regions contribute little to seismic radiation and, hence, may not be well resolved by the inversion procedures (Gusev, 2011; Razafindrakoto and Mai, 2014; Gallovic *et al.*, 2015). Second, we observe that the data points cluster at lower-slip values, whereas they are sparse at larger-slip values. Such an uneven distribution of data points can undermine the sensitivity of the upper tail to the goodness of fit. Therefore, we compute the goodness of fits emphasizing the upper tail of the distribution by considering only data points for slip greater than the average slip.

As goodness-of-fit metrics, we compute the coefficient of determination (R^2), the root mean square error (rmse), the mean absolute error (MAE), and the Akaike information criterion (AIC). In addition, we consider the variance reduction (Cohee and Beroza, 1994) to quantify the fits of the statistical distributions to the data, given by

$$\nabla\sigma^2 = 1 - \frac{\sum[y_i - f(u_i)]^2}{\sum y_i^2}, \tag{4}$$

in which y is the empirical probability, and $f(u)$ corresponds to the probability of slip u estimated using a specific statistical distribution. Given the general similarities of the distribution functions, it is necessary to rate them extensively to identify the overall best. To establish the needed statistical significance of the obtained fits, we examine the p values for the estimated values of rmse and MAE. To compute the p values, we generate 10,000 datasets of equal size, sampled randomly from the specific distribution, and then calculate the fraction of instances for which the fitted distribution performs better (Clauset *et al.*, 2009). We employ the inverse cumulative distribution function approach to sample random values for the truncated exponential distribution. The approach for sampling n random numbers from the truncated exponential distribution is as follows. For a random variable x drawn from a uniform distribution in the interval [0; 1], we obtain the corresponding value for the truncated exponential distribution as

$$u = F^{-1}(x, h, u_{\max}) = -\frac{1}{h}\log[1 - x(1 - \exp(-hu_{\max}))], \tag{5}$$

in which h is the rate parameter and $u_{\max}$ is the maximum value.

Implications of Spatial Smoothing

Finite-fault source inversions include spatial smoothing or regularization for stability, and to avoid oscillatory slip distributions. Typically, the amount of smoothing is defined by examining the trade-off between data misfit and model complexity (e.g., Sekiguchi *et al.*, 2000; Jónsson *et al.*, 2002; Fukuda and Johnson, 2008). Overfitting the data produces excessively complex models that are oscillatory and often physically unrealistic, but too strong smoothing degrades the fit to the data. Properly selected smoothing ensures that slip does not change drastically between adjacent points (e.g., Hartzell and Heaton, 1983). The optimal smoothing may be chosen based on statistical arguments (e.g., Akaike–Bayesian information criterion; Sekiguchi *et al.*, 2000), but often it is chosen by trial and error and therefore is subject to a potentially biased decision-making process.

The degree of smoothing influences the resulting slip model and by that also influences its probability distribution, an effect that we quantitatively investigate in the following. It is important to note that properly selected smoothing accounts for two important physical considerations: (1) the slip roughness should be consistent with observations of the roughness of exhumed slip surfaces (e.g., Candela *et al.*, 2011); (2) the stress change across the rupture plane needs to be finite, with reasonably bounded maximum stress-drop values (not exceeding ~100–200 MPa locally) and with average stress-drop values that are compatible with the range of measured far-field stress drops (~1–10 MPa, centered around 3 MPa).

We conduct a test by generating a synthetic slip distribution on a uniform grid of 18 km × 30 km with sampling of 0.5 km, using the von Karman ACF to compute the theoretical power spectrum of the 2D slip function. The von Karman ACF for 2D anisotropic case is given by

$$PS(k) = \frac{4\pi H}{K_H(0)}\frac{a_x a_z}{(1 + k^2)^{H+1}}, \tag{6}$$

in which K_H is the modified Bessel function of order H, a_x and a_z corresponds to the correlation lengths, and H is the Hurst exponent. This is combined with uniformly distributed random phase angles (under the condition of Hermitian symmetry) to describe the spatial correlation structure of slip in the Fourier domain. The Hurst exponent is chosen as $H = 0.5$, and we consider correlation lengths equal to 20% of the fault dimensions. The resulting spectral characterization is transformed into the spatial domain by inverse Fourier transformation. We then modify the probability distribution of slip so that it follows a lognormal distribution.

To emulate the spatial smoothing applied in source-inversion studies, we apply Laplacian smoothing (as described in the appendix of Jónsson *et al.*, 2002). We also consult Sekiguchi *et al.* (2000) to calibrate the varying degree of smoothing. Another test is conducted using slip models from the Source Inversion Validation (Mai *et al.*, 2016) exercises (see Data and Resources) for which the statistics of a known rupture model can be compared with inferred inversion solutions (Razafindrakoto *et al.*, 2015; Zhang *et al.*, 2015). The details of this analysis are given in Ⓔ Figures S1 and S2. We find that the inferred solutions can be described by the same statistical distribution as the true model but with varying scale and shape parameters.

Figure 2 displays examples of progressively smoothed slip maps, starting from very heterogeneous fault slip. The spatial smoothing introduces truncation effects at the upper

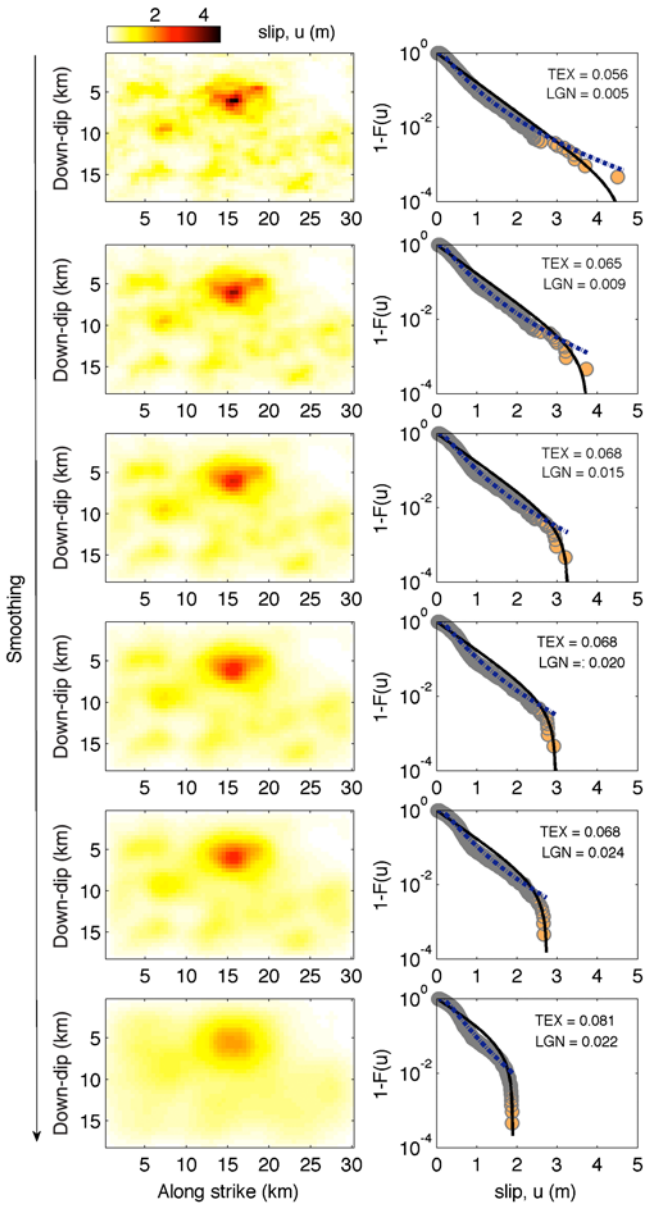

Figure 2. (Left) Progressively smoothed (from top to bottom) simulated slip distributions. (Right) CCDF of the slip distribution on the left with the dashed and solid lines depicting the fits of lognormal and truncated exponential distributions (notation as in Fig. 1b). The rmse values suggest that the lognormal distribution fits the data better than the truncated exponential distribution for all cases shown. The color version of this figure is available only in the electronic edition.

tail (resulting in a truncated distribution by reducing the maximum slip values) and also reduces the area over which low values of slip occur. However, we observe that the corresponding probability distributions are still better described by lognormal distribution than by truncated exponential distribution.

We also examine slip distributions obtained by varying degrees of smoothing for the 1995 Kobe earthquake (Sekiguchi *et al.*, 2000; their fig. 8). Also in this case, we observe that the lognormal distribution is consistently observed for the differently smoothed models (Ⓔ Fig. S3). For strongly smoothed slip distributions, the probability distribution of slip is better described by a truncated lognormal rather than by a truncated exponential distribution. Furthermore, we find that the spatial features of the slip distributions remain relatively robust over the range of moderate smoothing (Ⓔ Fig. S4). These observations suggest that typical spatial smoothing applied in source-inversion studies does not greatly affect the resulting probability distribution of slip.

The impact of smoothing is also evident when examining the spatial distribution of stress changes on the rupture plane (Ⓔ Figs. S5–S7). Moderate smoothing, as typically applied by the source inversions, constrains the overall stress drop, eliminates unrealistically large stress drop dispersed over the rupture plane, and results in average stress drop consistent with previous estimations (e.g., Fletcher and McGarr, 2006).

Results and Discussions

Truncated Exponential Probability Distribution of Slip

Let us first examine the average probability distribution of slip. The scaling relationships between slip areas ($u > u_i$) and seismic moment allow computing the average complementary cumulative distributions of slip. Figure 3 provides an overview of the scaling relationships. Details of the regression analyses are given in Ⓔ Figures S8–S12. We observe that the coefficient of determination R^2 and the correlation coefficient r are typically above 0.70. The estimated values for the slope (β in equation 3) between slip area and seismic moment are stable across different slip bins and for each subset of rupture models. These scaling relationships show that reverse dip-slip earthquakes follow self-similar scaling, with $\beta \sim 2/3$. For strike-slip and normal dip-slip earthquakes, we observe a deviation from self-similarity. Because seismic moment M_0 and rupture area A (equals WL) are related by M_0 equal to $\mu W L u_{\text{avg}}$, in which μ is shear modulus, u_{avg} is average slip, L is fault length, and W is fault width, a slope of $\beta = 2/3$ in area–moment scaling indicates self-similar earthquake source scaling (Kanamori and Anderson, 1975). Self-similar in this context means that changing M_0 by a factor γ requires proportional changes of each physical parameter (W, L, u_{avg}) by $\gamma/3$, hence $L \sim M_0^{1/3}$, $W \sim M_0^{1/3}$, and, consequently, $A \sim M_0^{2/3}$. Self-similar earthquake source scaling is also associated with the generally observed scale-invariant stress drop ($\Delta\sigma \sim 3$ MPa). Previous studies reported difference in source scaling between strike-slip and reverse dip-slip events (e.g., Stock and Smith, 2000; Hanks and Bakun, 2002; Mai and Beroza, 2002; Hanks and Bakun, 2008) but not for normal dip-slip events. However, detailed investigations on the source scaling is beyond the scope of the present study.

Figure 4 depicts the average probability distribution of slip, separated by faulting regimes and constructed using the scaling relationships (Fig. 3). By fitting the different statistical distributions (Table 1), we observe that the truncated exponential distribution best describes the overall shape of the probability distributions. The truncated exponential

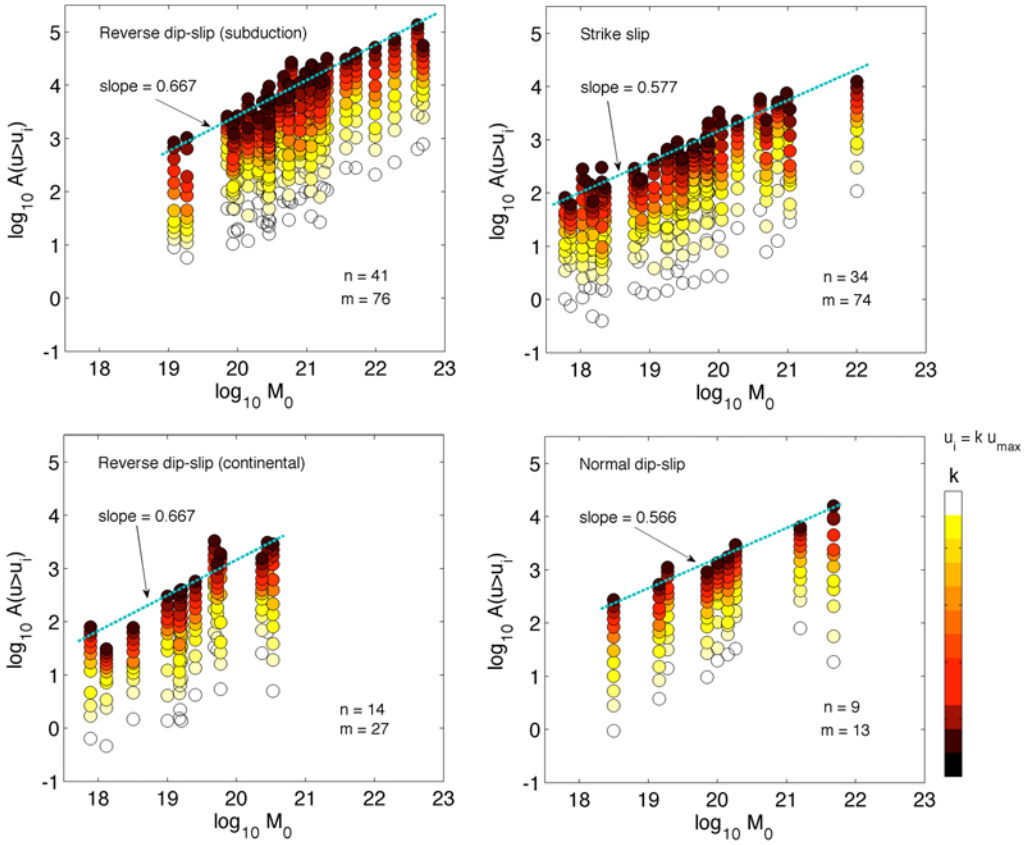

Figure 3. Seismic moment M_0 (in N·m) versus slip area A (in km^2), considering rupture models of earthquakes grouped in different faulting regimes. Slip u_i is equal to a fraction k of maximum slip $u_{\max}$ and is chosen to be centered at each 12 uniform bins. In case multiple models exist for a given event, we use the mean of the logarithm-transformed data in the regression analyses. In each panel, n denotes the number of events, and m indicates the number of models. The line denotes the slope, which we find to be robust statistically across the different slip areas in each group. The color version of this figure is available only in the electronic edition.

probability distribution for nonnegative slip u is defined in terms of the complementary cumulative distribution as

$$1 - F(u) = \frac{\exp(-\frac{u}{u_c}) - \exp(-\frac{u_{\max}}{u_c})}{1 - \exp(-\frac{u_{\max}}{u_c})}. \qquad (7)$$

The parameters u_c and $u_{\max}$ are the scale parameter and the maximum slip, respectively (see Table 1 for an alternate definition). The distribution in equation 7 constitutes an exponential decay, truncated at the upper tail, that yields reduced probabilities for very large slip compared with the exponential trend. Accordingly, we can identify the largest slip u_t at which the probabilities start deviating from the exponential decay (Figs. 1b and 4). We will later discuss the significance of this parameter.

To further analyze the fitting of the considered distributions for individual rupture models, we generate Q–Q plots (Fig. 5 and Ⓔ Fig. S13). These indicate that the truncated exponential distribution consistently best fits the slip probabilities. The advantage of the truncated exponential distribution is seen particularly in the upper tails of the distributions. This observation is well supported by the analysis of the goodness-of-fit measures for the investigated rupture models (Ⓔ Tables S2–S6).

By constructing the probability distribution using the described slip-area scaling approach, we follow a strategy similar to generating frequency statistics (also referred to as relative frequency or empirical probability). For illustration, Figure 6 displays the distributions using normalized histograms and directly calculated CCDFs, including the fits of the different statistical distributions. The histograms do not reveal the differences between the upper tails of the different fits, whereas the CCDFs clearly indicate that the truncated exponential distribution is the best-fitting distribution.

We then quantify the goodness of fit and identify the best-fitting statistical distribution for the entire database by evaluating the number (or percentage) of rupture models associated with certain goodness-of-fit values (indicative of good-to-excellent fit). For instance, a variance reduction of 95.0%–99.9% is much more frequently observed for the truncated exponential distribution than for any other of the considered statistical distributions (Fig. 7a). For fits with $R^2 > 90$, the truncated exponential distribution accounts for 85% of the models, the exponential distribution accounts for 74%, the Weibull distribution accounts for 67%, the Gamma distribution accounts for 73%, and the lognormal distribution accounts for only 38% of the models. The rmse values are

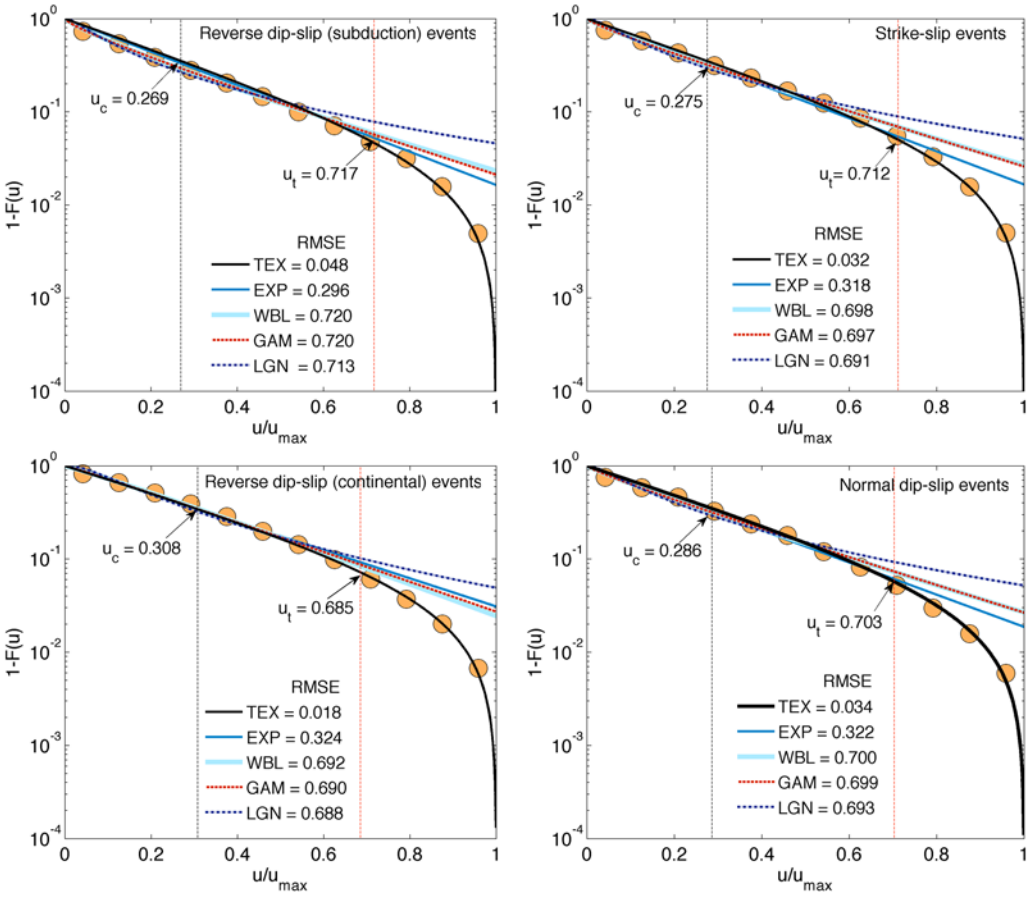

Figure 4. Average probability distributions of slip. The dots denote the average CCDF of slip, calculated using scaling relationships between seismic moment and slip areas. The four panels show the results for different faulting regimes. The curves represent the fits of statistical distributions considered in this study (notations as in Fig. 1). The color version of this figure is available only in the electronic edition.

found to be smaller for the truncated exponential distribution (Fig. 7b); a similar observation can be made for MAE values (Fig. 7c). Additionally, smaller AIC values are found for the truncated exponential distribution than for the other statistical distributions (Fig. 7d). In summary, the various goodness-of-fit measures confirm that the probability distribution of slip, especially in its upper tails, is best described by the truncated exponential distribution.

Similar results are obtained considering different subsets of the rupture-model data. Figure 8 depicts the number of rupture models observed with a range of variance reductions when fitting different statistical distributions to the data subsets. In all cases, the number of rupture models that are better fit by the truncated exponential distribution is consistently larger. Because our results do not depend on inversion method or data used for the slip inversions, we consider them robust and generally applicable. The truncated exponential distributions are associated with fits that show p values of 0.1 or higher for 90% of the investigated rupture models (Ⓔ Table S2). This high statistical significance suggests excellent data fitting and corroborates the finding that the truncated exponential distribution best characterizes the slip heterogeneity associated with earthquake ruptures.

Scaling of Probability Distribution

To examine the variability of the probability distributions with earthquake magnitude, we develop relationships between the average slip and the best-fitting parameters of the truncated exponential distribution. For the regression analyses, we select only those rupture models that are consistent with the truncated exponential distribution, as indicated by p value ≥ 0.1. Additionally, we exclude six models found to have significantly limited amount of low (near-zero) slip. These models can be associated with either fast finite-fault inversion technique (unpublished online models), limited data used to image the rupture process, or excessive simplification of complex fault geometry. Figure 9 depicts the regression analyses. It can be seen that the scale parameter of the best-fitting truncated exponential distribution and maximum slip correlates well with average slip.

The observed scaling property of the probability distribution of slip is a result of the space–time complexity of the rupture process that is driven by nonlinear earthquake source dynamics. First, both the spatial bounds of the rupture, as well as roughness features of internal fault surface, generate healing waves that limit the slip (Heaton, 1990; Beroza and Mikumo, 1996; Shi and Day, 2013). Second, the spatiotemporal growth of earthquake

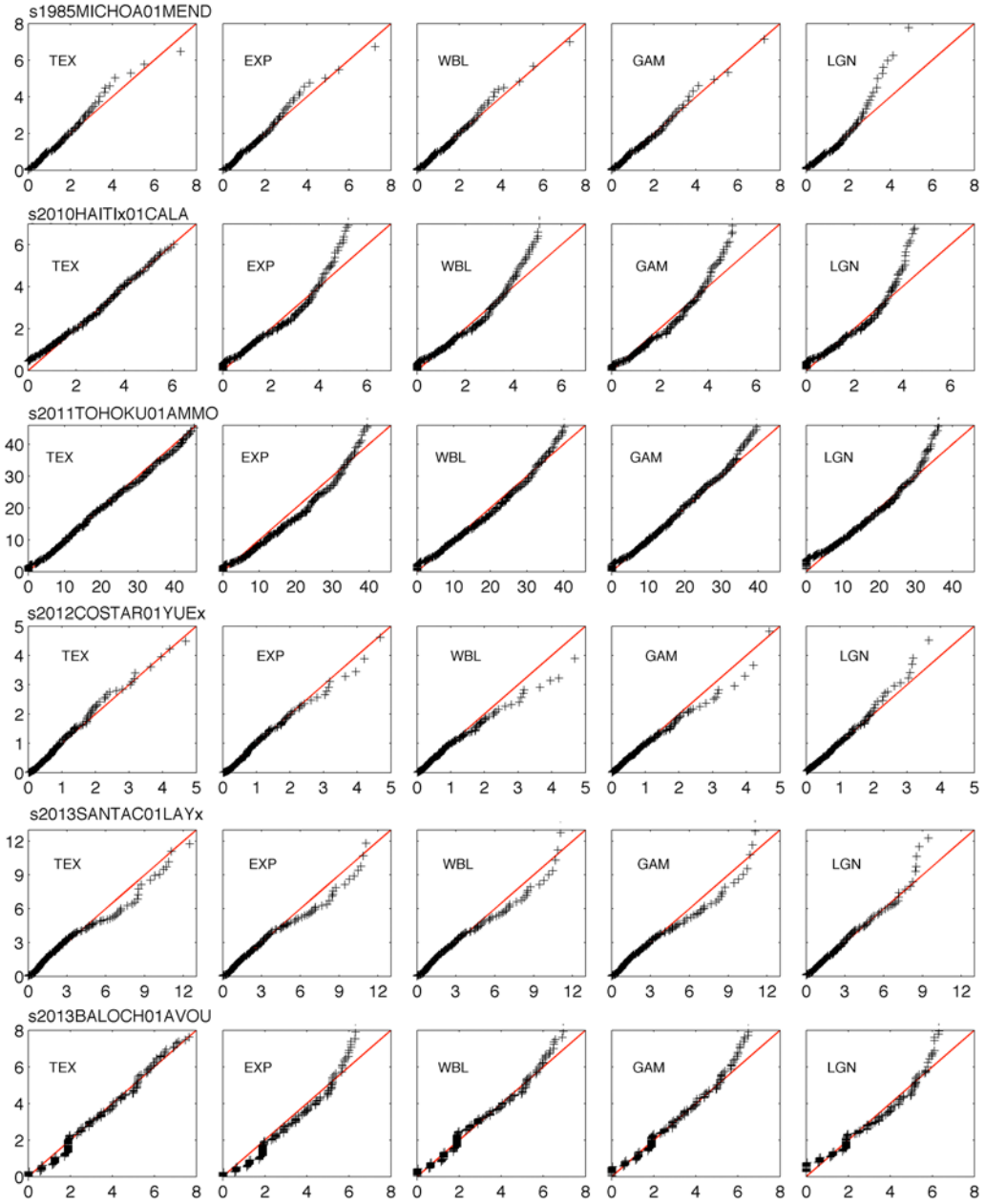

Figure 5. *Q–Q* plots illustrating the fits of the considered statistical distributions to the data for a few selected rupture models. Each model is indicated with the event tag used in the SRCMOD database. In each panel, the ordinate shows quantiles for the empirical slip values, and the abscissa displays the corresponding values for the assumed statistical distributions. In each panel, points located on the 45° reference line indicate a perfect agreement with data and empirical distribution. The color version of this figure is available only in the electronic edition.

rupture is controlled by nonuniform stress and strength conditions of the fault, which influence the slip heterogeneity (Day *et al.*, 1998; Madariaga *et al.*, 1998; Guatteri *et al.*, 2003). Third, empirical studies have shown that rupture area scales with average slip, independent of earthquake magnitude (e.g., Mai and Beroza, 2000; Blaser *et al.*, 2010; Leonard, 2010).

Implications of Truncated Exponential Slip Distribution

The average probability distributions as well as the analysis of individual rupture models corroborate that the truncated exponential distribution best characterizes the empirical distributions of earthquake slip. This evidence contradicts previous investigations of the slip probability distribution. Gusev (2011) hypothesized that the slip distribution follows a log-normal distribution, whereas Lavallée *et al.* (2006) proposed a non-Gaussian Lévy law (i.e., a distribution with a power-law decay of the upper tail) for slip heterogeneity. The mismatch becomes particularly visible when examining the occurrence of larger-slip values, because they define the upper tails of the empirical distributions and hence resolve the best-fitting statistical distribution.

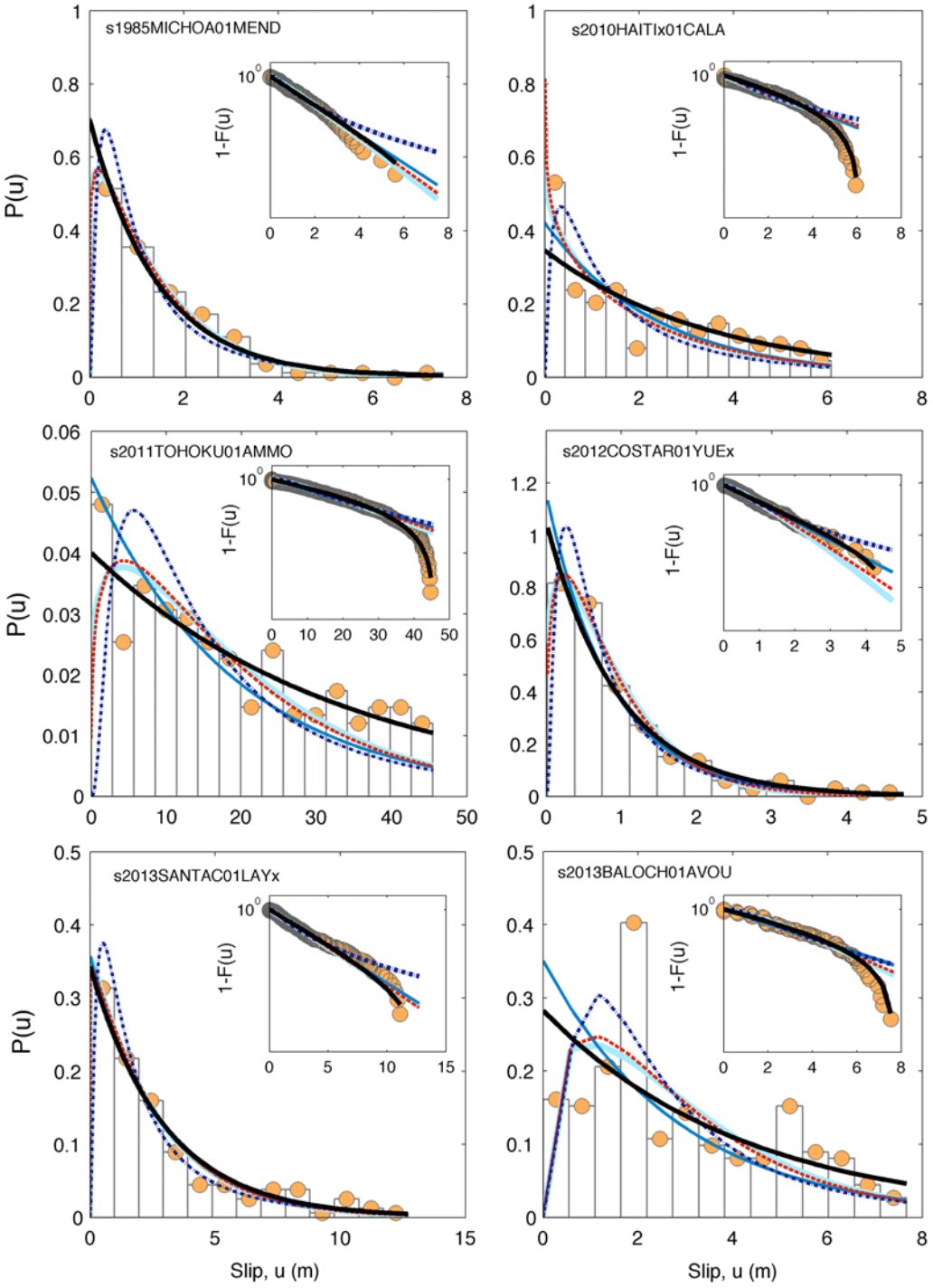

Figure 6. The probability distribution of slip for six exemplary rupture models, represented by normalized histograms. $P(u)$ is the probability for the slip centered at each bin (dots). The number of bins, in each case, is given by $\sqrt{n}$, in which n is total number of data points. Insets display the CCDF. Fits of different statistical distribution are also depicted (legends are same as in Fig. 1), with the truncated exponential distribution shown by the black solid curves. The color version of this figure is available only in the electronic edition.

The truncated exponential probability distribution is consistent with large fault-surface regions of low slip but limited zones of large slip and thus has an immediate relevance for rupture physics. This characteristic of earthquake ruptures can be linked to prerupture stresses on the fault being spatially variable with highly localized areas of large stress. Deviations from this general behavior are observed for some rupture models that are characterized either by small low-slip regions or by excessively large areas of (near) zero slip. We attribute these to aberrations in the source-imaging process, due to the limited sensitivity of source inversions to fault regions of low-seismic radiation and the resulting inability of

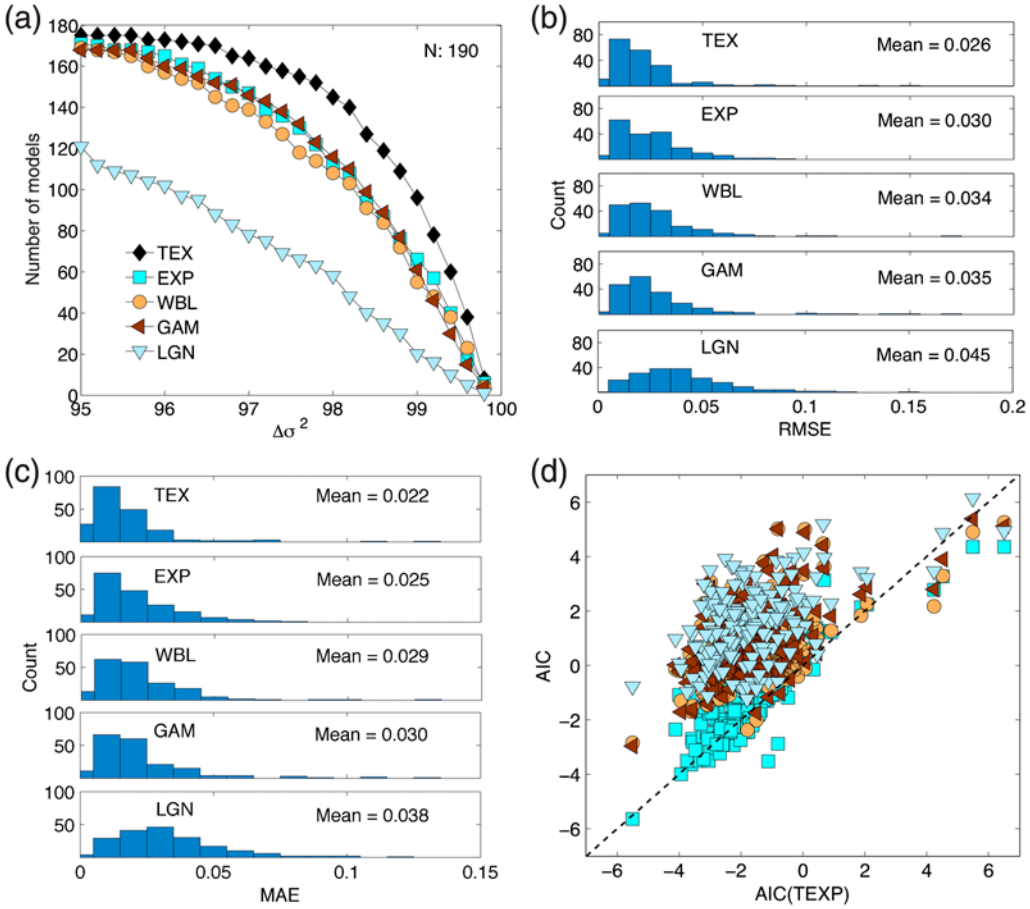

Figure 7. (a) Number of models corresponding to greater or equal value of variance reduction $\nabla\sigma^2$ for different statistical distributions (notations as in Fig. 1b). *N* refers to total number of models. (b) Histograms of rmse values for the fits of the different statically distributions. (c) Histograms of mean absolute error (MAE) values for the fits of the different statically distributions. (d) Cross plot between values of the Akaike information criterion (AIC) obtained for fits of truncated exponential distribution and those for the other distributions, indicating that the TEX-distribution performs better in explaining the data (most points fall above the dashed line that indicates identical AIC values; lower AIC value is better). The color version of this figure is available only in the electronic edition.

the data to effectively resolve low-slip values (e.g., Razafindrakoto and Mai, 2014). In contrast, we associate lower uncertainty to the (spatially limited) zones of larger slip, as they are well detectable in source inversions.

Fault strength, the acting stresses in the rock volume surrounding the rupture plane, as well as the dynamically evolving frictional fault properties during sliding, impose an upper limit to the maximum slip. Constraints on the largest slip are also related to finite strain energy that can be stored in the fault systems and to consolidated zones that act as barriers to the rupture, or to both. This phenomenon is analogous to the limits on the maximum magnitude in frequency–magnitude distributions of earthquakes, for which truncated exponential distribution is often used to approximate the Gutenberg–Richter law (Cosentino *et al.*, 1977; Raschke, 2015). We point out that this analogy does not apply to fault-specific seismicity that may exhibit a characteristic-earthquake behavior with increased probabilities of larger magnitude compared to an exponential decay (e.g., Wesnousky, 1994). Furthermore, an upper limit on maximum slip precludes unphysical stress changes (e.g., Andrews, 1980; Bouchon *et al.*, 1998; Ripperger and Mai, 2004; Bailey and Ben-Zion, 2009). Thus, the reduced probabilities of very large slip (implied by truncation of the exponential decay) are a consequence of earthquake-rupture physics that imposes physical limits on the maximum slip.

The truncated exponential probability distribution also characterizes the observed slip heterogeneity. We classify the slip distribution using the parameters u_c and u_t (Figs. 1b and 4), in which u_c is related to the expected value of the distribution and u_t is controlled by, but is typically less than, the truncation point (maximum slip) of the distribution. These parameters provide a natural demarcation of the slip range: low-to-moderate values, large values, and largest-slip values with higher probabilities, average probabilities, and lower probabilities. Accordingly, we associate large- and largest-slip asperities with slip u in the ranges $u_c \leq u < u_t$ and $u_t \leq u$. This quantification of slip asperities, or slip heterogeneity, is statistically better justified than previous definitions of slip asperities, for example, fault patches with slip $u > 1.5u_{\text{avg}}$ (Somerville *et al.*, 1999). Further-

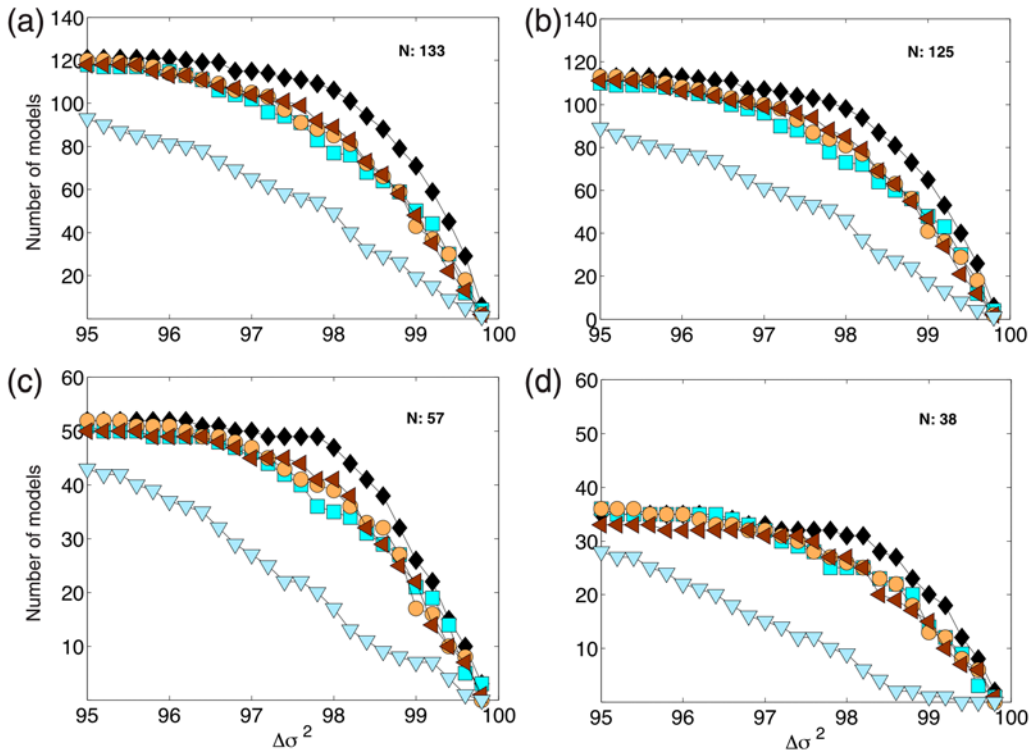

Figure 8. Same as Figure 7a but for different selection criteria on the database: (a) all models but excluding fast finite-fault models; (b) all models excluding fast finite-fault and geodetic models; (c) joint-inversion models only; (d) joint-inversion models excluding those with nonzero slip. *N* refers to total number of models. The color version of this figure is available only in the electronic edition.

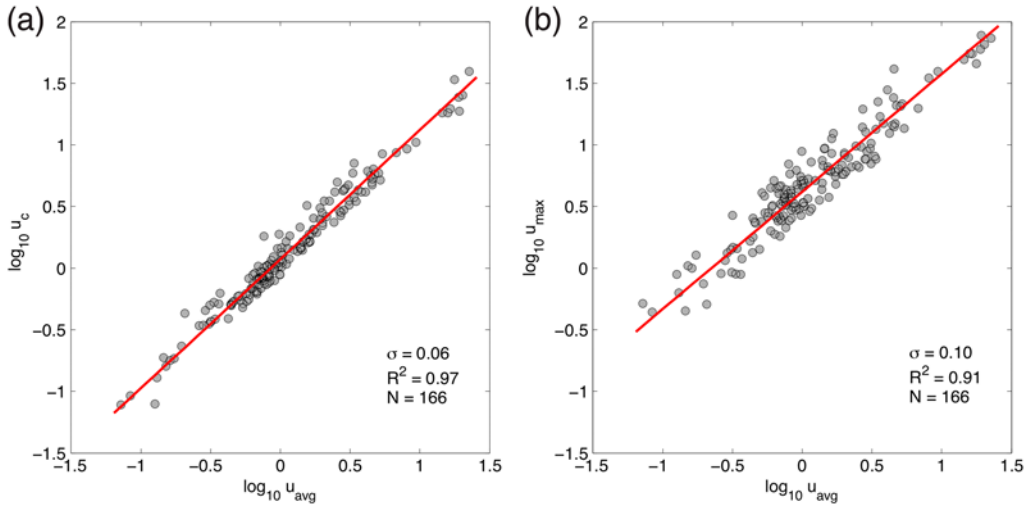

Figure 9. (a) Relationship between the scale parameter u_c (in m) of the best-fitting truncated exponential distribution and average slip, u_{avg} (in m). The line shows the linear fit given by $\log_{10} u_c = 1.05 \log_{10} u_{avg} + 0.07$. R^2 and N denote the coefficient of determination and the number of data points. (b) The scaling of maximum slip u_{max} (in m) with respect to the average slip. The linear fit yields $\log_{10} u_{max} = 0.95 u_{avg} + 0.62$, $\sigma = 0.10$. The color version of this figure is available only in the electronic edition.

more, this classification is more consistent with the slip variability across different events than that proposed by Mai *et al.* (2005), who defined large and very-large-slip asperities as given by $1/3\ u_{max} \le u < 2/3 u_{max}$, and by $2/3 u_{max} \le u$, in which u_{max} is maximum slip. Interestingly, the estimated average values of u_c and u_t (Fig. 4) roughly agree with the empirically defined ranges specified by Mai *et al.* (2005).

Because stress and strength conditions are generally not identical for different earthquakes, the rupture processes inferred in source inversions reveal significant variation between events. This interevent difference is captured by the variability of the probability distribution of slip. We classify this variability into three broad categories: (1) absence of large-slip asperities ($u_c \ge u_t$), (2) clear demarcation between large

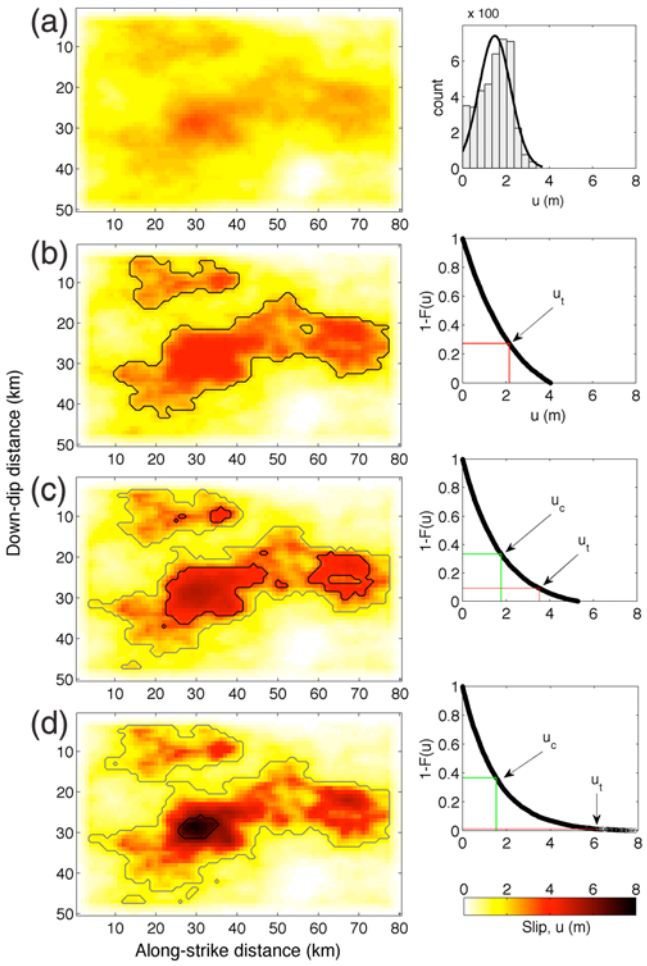

Figure 10. (a) A rupture scenario with quasi-normal distributed slip (as depicted in the right plot). (b) Same as (a) but the slip distribution is now transformed using the truncated exponential distribution and has largest-slip asperities (darker contour) but no large-slip asperities. The right plot depicts the CCDF of the slip with the lines indicating scale parameter u_c, and largest slip u_t, at which the probabilities start deviating from the exponential decay. (c) Same as (b) but large-slip (lighter contour) and largest-slip asperities are well demarcated. (d) Same as (b) but the slip distribution is dominated by large-slip asperities. The color version of this figure is available only in the electronic edition.

and largest-slip asperities ($u_c < u_t < u_{\max}$), and (3) paucity of largest-slip asperities ($u_c < u_t \sim u_{\max}$). The first two cases imply very strong and strong physical constraints on the largest slip (subcritical behavior), which may downsize and even eliminate large-slip asperities. The last case implies paucity of largest-slip asperities (near-critical behavior) in the slip distributions. Because the existence of slip asperities is related to nonuniform strength conditions on the fault (Miyatake, 1992; Mai *et al.*, 2005), the properties and parameters of the truncated exponential probability distribution may help to further quantify strength and stress heterogeneity on earthquake faults.

Our findings have significant implications for generating rupture scenarios for physics-based ground-motion simulations. If kinematic or pseudodynamic source characterizations are used (e.g., Guatteri *et al.*, 2004; Liu *et al.*, 2006; Mena *et al.*, 2012), the on-fault slip pattern can be specified in a more physically self-consistent way. If spontaneous dynamic rupture simulations are carried out, the initial stress distribution can be constrained based on our results, whereas the resulting kinematic rupture process can be validated against the observed truncated exponential distribution of slip. Apart from the slip values on the rupture plane, a kinematic rupture model requires the hypocentral location, source time function, the rise time (duration of slip at each point of the fault), the rupture-onset time, and the rake (angle of slip direction) to describe the spatiotemporal evolution of the earthquake rupture. Several studies have attempted to illuminate the properties of and correlation between these parameters (e.g., Guatteri *et al.*, 2004; Mai *et al.*, 2005; Graves and Pitarka, 2010; Schmedes *et al.*, 2010; Mena *et al.*, 2012; Song *et al.*, 2013). Delivering physically consistent scenario ruptures that incorporate the important characteristics of dynamic ruptures is a key research objective for accurate ground-motion simulations.

The present study focuses on the distribution of earthquake slip, aiming to develop a simple yet physically consistent approach to parameterize slip heterogeneity in the generation of rupture scenarios. As an illustration, we generate examples of rupture scenarios that visualize the variability of slip heterogeneity for a hypothetical M_w 7.5 reverse-faulting earthquake. Because of identical rupture dimensions, these rupture scenarios share the same average slip. We enforce identical spatial structure of slip (using the van Karman ACF in equation 6 and identical correlation parameters a_x, a_z, and H, as well as keeping the random phase angles fixed). The slip distributions are scaled to an average slip that produces the desired seismic moment. The initial slip distribution has a quasi-normal probability distribution (Fig. 10a). Subsequently, we modify the probability distribution of the slip so that it follows the truncated exponential distribution, and accordingly, the maximum slip on the fault is changed. We apply different parameter choices of the distribution to generate the mentioned three categories of slip heterogeneity. Thus, we have three synthetic rupture models to examine the variability of slip heterogeneity: a case of very strong physical constraints on the maximum slip (Fig. 10b), a typical scenario (Fig. 10c), and a case of weak physical constraints on the maximum slip (Fig. 10d). In these examples, the total area of slip asperities increases with increasing maximum slip, whereas the area of the largest-slip asperities reduces with increasing maximum slip. These statistical simulations illustrate how the probability distribution of slip allows modeling the slip heterogeneity for any particular earthquake rupture.

Conclusions

We show that the truncated exponential distribution best describes the probability distribution of coseismic earthquake slip on the rupture plane. The observed slip distributions are consistent with physical constraints on largest slip. We establish that the probability distribution facilitates a simple classification and quantification of slip asperities, consistent

with nonuniform spatiotemporal stress and strength conditions across the fault. Because the parameters of the probability distribution function scale with the average slip, we infer that probability distribution of earthquake slip is physically linked to the rupture dimensions, because the average slip is determined by the total rupture area. Our analysis thus provides strong observational constraints on the slip heterogeneity and, consequently, allows for more realistic modeling of earthquake-rupture scenarios to improve physics-based ground-motion simulations for seismic- and tsunami-hazard calculations.

Data and Resources

The rupture models used in this study were extracted from the SRCMOD database (http://equake-rc.info/srcmod, last accessed March 2016). The Source Inversion Validation (SIV) project is accessible at http://equake-rc.info/siv (last accessed March 2016). MATLAB scripts developed for this present study can be downloaded from the equake-rc website (http://equake-rc.info/CERS-software/, last accessed March 2016).

Acknowledgments

We thank all contributors to the SRCMOD database and all the participants of the Source Inversion Validation (SIV) project. M. Galis and J. Vyas are acknowledged for helpful discussions. We also thank S. Wesnousky and O. Zielke for reviewing an early version of the article. Careful and constructive comments by Associate Editor T. Pratt and two anonymous reviewers helped to improve the article. Research reported in this publication is supported by the King Abdullah University of Science and Technology (KAUST), baseline funding BAS/1339-01-01 and Competitive Research Grant URF/1/2160-01-01.

References

Andrews, D. J. (1980). A stochastic fault model: 1. Static case, *J. Geophys. Res.* **85,** 3867–3877.

Bailey, I. W., and Y. Ben-Zion (2009). Statistics of earthquake stress drops on a heterogeneous fault in an elastic half-space, *Bull. Seismol. Soc. Am.* **99,** 1786–1800.

Basu, B., D. Tiwari, D. Kundu, and R. Prasad (2009). Is Weibull distribution the most appropriate statistical strength distribution for brittle materials? *Ceram. Int.* **35,** 237–246.

Beroza, G. C., and T. Mikumo (1996). Short slip duration in dynamic rupture in the presence of heterogeneous fault properties, *J. Geophys. Res.* **101,** 22,449–22,460.

Bertalan, Z., A. Shekhawat, J. P. Sethna, and S. Zapperi (2014). Fracture strength: Stress concentration, extreme value statistics, and the fate of the Weibull distribution, *Phys. Rev. Appl.* **2,** 034008.

Blaser, L., F. Krüger, M. Ohrnberger, and F. Scherbaum (2010). Scaling relations of earthquake source parameter estimates with special focus on subduction environment, *Bull. Seismol. Soc. Am.* **100,** 2914–2926.

Bouchon, M., M. Campillo, and F. Cotton (1998). Stress field associated with the rupture of the 1992 Landers, California, earthquake and its implications concerning the fault strength at the onset of the earthquake, *J. Geophys. Res.* **103,** 21,091–21,097.

Bracewell, R. N. (1986). *The Fourier Transform and Its Applications*, Second Ed., McGraw-Hill, New York.

Candela, T., F. Renard, J. Schmittbuhl, M. Bouchon, and E. E. Brodsky (2011). Fault slip distribution and fault roughness, *Geophys. J. Int.* **187,** 959–968.

Causse, M., L. A. Dalguer, and P. M. Mai (2013). Variability of dynamic source parameters inferred from kinematic models of past earthquakes, *Geophys. J. Int.* **196,** 1754–1769.

Clauset, A., C. R. Shalizi, and M. E. Newman (2009). Power-law distributions in empirical data, *SIAM Rev.* **51,** 661–703.

Cohee, B. P., and G. C. Beroza (1994). A comparison of two methods for earthquake source inversion using strong motion seismograms, *Ann. Geophys.* **37,** 1515–1538.

Cosentino, P., V. Ficarra, and D. Luzio (1977). Truncated exponential frequency–magnitude relationship in earthquake statistics, *Bull. Seismol. Soc. Am.* **67,** 1615–1623.

Day, S. M. (1982). Three-dimensional simulation of spontaneous rupture: The effect of nonuniform prestress, *Bull. Seismol. Soc. Am.* **72,** 1881–1902.

Day, S. M., G. Yu, and D. J. Wald (1998). Dynamic stress changes during earthquake rupture, *Bull. Seismol. Soc. Am.* **88,** 512–522.

Dunham, E. M., D. Belanger, L. Cong, and J. E. Kozdon (2011). Earthquake ruptures on rough faults, in *Multiscale and Multiphysics Processes in Geomechanics (results of workshop at Stanford Univ., June, 2010)*, R. I. Borja (Editor), Springer Series in Geomechanics and Geoengineering, ISBN: 978-3-642-19629-4, 145–148.

Fang, Z., and E. M. Dunham (2013). Additional shear resistance from fault roughness and stress levels on geometrically complex faults, *J. Geophys. Res.* **118,** 3642–3654.

Fletcher, J. B., and A. McGarr (2006). Distribution of stress drop, stiffness and fracture energy over earthquake rupture zones, *J. Geophys. Res.* **111,** no. B03312, doi: 10.1029/2004JB003396.

Freedman, D., and P. Diaconis (1981). On the histogram as a density estimator: L 2 theory, *Probab. Theor. Relat. Field.* **57,** 453–476.

Fukuda, J. I., and K. M. Johnson (2008). A fully Bayesian inversion for spatial distribution of fault slip with objective smoothing, *Bull. Seismol. Soc. Am.* **98,** 1128–1146.

Fuller, W. A. (1987). *Measurement Error Models*, John Wiley & Sons, New York.

Gallovič, F., W. Imperatori, and P. M. Mai (2015). Effects of three-dimensional crustal structure and smoothing constraint on earthquake slip inversions: Case study of the M_w 6.3 2009 L'Aquila earthquake, *J. Geophys. Res.* **120,** 428–449.

Goda, K., P. M. Mai, T. Yasuda, and N. Mori (2014). Sensitivity of tsunami wave profiles and inundation simulations to earthquake slip and fault geometry for the 2011 Tohoku earthquake, *Earth Planets Space* **66,** 1–20.

Graves, R. W., and A. Pitarka (2010). Broadband ground-motion simulation using a hybrid approach, *Bull. Seismol. Soc. Am.* **100,** 2095–2123.

Guatteri, M., P. M. Mai, and G. C. Beroza (2004). A pseudo-dynamic approximation to dynamic rupture models for strong ground motion prediction, *Bull. Seismol. Soc. Am.* **94,** 2051–2063.

Guatteri, M., P. M. Mai, G. C. Beroza, and J. Boatwright (2003). Strong ground-motion prediction from stochastic-dynamic source models, *Bull. Seismol. Soc. Am.* **93,** 301–313.

Gusev, A. A. (2011). Statistics of the values of a normalized slip in the points of an earthquake fault, *Izvestiya Phys. Solid Earth* **47,** 176–185.

Hanks, T. C., and W. H. Bakun (2002). A bilinear source-scaling model for M-log A observations of continental earthquakes, *Bull. Seismol. Soc. Am.* **92,** 1841–1846.

Hanks, T. C., and W. H. Bakun (2008). M-log A observations of recent large earthquakes, *Bull. Seismol. Soc. Am.* **98,** 490–494.

Hartzell, S. H., and T. H. Heaton (1983). Inversion of strong ground motion and teleseismic waveform data for the fault rupture history of the 1979 Imperial valley, California, earthquake, *Bull. Seismol. Soc. Am.* **73,** 1553–1583.

Heaton, T. H. (1990). Evidence for and implications of self-healing pulses of slip in earthquake rupture, *Phys. Earth Planet. In.* **64,** 1–20.

Heimpel, M. (1996). Earthquake size-frequency relations from an analytical stochastic rupture model, *J. Geophys. Res.* **101,** 22,435–22,448.

Jónsson, S., H. Zebker, P. Segall, and F. Amelung (2002). Fault slip distribution of the 1999 M_w 7.1 Hector Mine, California, earthquake, estimated from satellite radar and GPS measurements, *Bull. Seismol. Soc. Am.* **92,** 1377–1389.

Kagan, Y. Y. (2005). Earthquake slip distribution: A statistical model, *J. Geophys. Res.* **110,** no. B05S11, doi: 10.1029/2004JB003280.

Kanamori, H., and D. L. Anderson (1975). Theoretical basis of some empirical relations in seismology, *Bull. Seismol. Soc. Am.* **65,** 1073–1095.

Krumbholz, M., C. F. Hieronymus, S. Burchardt, V. R. Troll, D. C. Tanner, and N. Friese (2014). Weibull-distributed dyke thickness reflects probabilistic character of host-rock strength, *Nat. Comm.* **5,** doi: 10.1038/ncomms4272.

Lavallée, D., P. Liu, and R. J. Archuleta (2006). Stochastic model of heterogeneity in earthquake slip spatial distributions, *Geophys. J. Int.* **165,** 622–640.

Leonard, M. (2010). Earthquake fault scaling: Self-consistent relating of rupture length, width, average displacement, and moment release, *Bull. Seismol. Soc. Am.* **100,** 1971–1988.

Lienhard, J. H., and P. L. Meyer (1967). A physical basis for the generalized gamma distribution, *Q. Appl. Math.* **25,** 330.

Liu, P., R. J. Archuleta, and S. H. Hartzell (2006). Prediction of broadband ground-motion time histories: Hybrid low/high-frequency method with correlated random source parameters, *Bull. Seismol. Soc. Am.* **96,** 2118–2130.

Lobo-Guerrero, S., and L. E. Vallejo (2006). Application of Weibull statistics to the tensile strength of rock aggregates, *J. Geotech. Geoenviron. Eng.* **132,** 786–790.

Madariaga, R., K. Olsen, and R. Archuleta (1998). Modeling dynamic rupture in a 3D earthquake fault model, *Bull. Seismol. Soc. Am.* **88,** 1182–1197.

Mai, P. M., and G. C. Beroza (2000). Source scaling properties from finite-fault-rupture models, *Bull. Seismol. Soc. Am.* **90,** 604–615.

Mai, P. M., and G. C. Beroza (2002). A spatial random field model to characterize complexity in earthquake slip, *J. Geophys. Res.* **107,** 1978–2012.

Mai, P. M., and K. K. S. Thingbaijam (2014). SRCMOD: An online database of finite-fault rupture models, *Seismol. Res. Lett.* **85,** 1348–1357.

Mai, P. M., D. Schorlemmer, M. Page, J.-P. Ampuero, K. Asano, M. Causse, S. Custodio, W. Fan, G. Festa, M. Galis, *et al.* (2016). The earthquake-source inversion validation (SIV) project, *Seismol. Res. Lett.* **87,** no. 3, doi: 10.1785/0220150231.

Mai, P. M., P. Somerville, A. Pitarka, L. Dalguer, S. Song, G. Beroza, H. Miyake, and K. Irikura (2006). On scaling of fracture energy and stress drop in dynamic rupture models: Consequences for near-source ground-motions, in *Earthquakes: Radiated Energy and the Physics of Faulting*, Vol. 170, Geophysical Monograph Series, American Geophysical Union, 283–293.

Mai, P. M., P. Spudich, and J. Boatwright (2005). Hypocenter locations in finite-source rupture models, *Bull. Seismol. Soc. Am.* **95,** 965–980.

Mena, B., L. A. Dalguer, and P. M. Mai (2012). Pseudodynamic source characterization for strike-slip faulting including stress heterogeneity and super-shear ruptures, *Bull. Seismol. Soc. Am.* **102,** 1654–1680.

Miyatake, T. (1992). Dynamic rupture processes of inland earthquakes in Japan weak and strong asperities, *Geophys. Res. Lett.* **19,** no. 10, 1041–1044, doi: 10.1029/92GL01046.

Oglesby, D. D., and P. M. Mai (2012). Fault geometry, rupture dynamics, and ground motion from potential earthquakes on the North Anatolian fault zone under the Sea of Marmara, *Geophys. J. Int.* **188,** no. 3, 1071–1087, doi: 10.1111/j.1365-246X.2011.05289.x.

Oglesby, D. D, P. M. Mai, K. Atakan, and S. Pucci (2008). Dynamic models of earthquakes on the North Anatolian fault under the Sea of Marmara: The effect of hypocenter location, *Geophys. Res. Lett.* **35,** L18302, doi: 10.1029/2008GL035037.

Ramírez-Gaytán, A., J. Aguirre, M. A. Jaimes, and V. Huérfano (2014). Scaling relationships of source parameters of M_w 6.9–8.1 earthquakes in the Cocos–Rivera–North American subduction zone, *Bull. Seismol. Soc. Am.* **104,** 840–854.

Raschke, M. (2015). Modeling of magnitude distributions by the generalized truncated exponential distribution, *J. Seismol.* **19,** 265–271.

Razafindrakoto, H. N., and P. M. Mai (2014). Uncertainty in earthquake source imaging due to variations in source time function and Earth structure, *Bull. Seismol. Soc. Am.* **104,** 855–874.

Razafindrakoto, H. N., P. M. Mai, M. G. Genton, L. Zhang, and K. K. S. Thingbaijam (2015). Quantifying variability in earthquake rupture models using multidimensional scaling: Application to the 2011 Tohoku earthquake, *Geophys. J. Int.* **202,** 17–40.

Ripperger, J., and P. M. Mai (2004). Fast computation of static stress changes on 2D faults from final slip distributions, *Geophys. Res. Lett.* **31,** L18610, doi: 10.1029/2004GL020594.

Schmedes, J., R. J. Archuleta, and D. Lavallée (2010). Correlation of earthquake source parameters inferred from dynamic rupture simulations, *J. Geophys. Res.* **115,** no. B03304, doi: 10.1029/2009JB006689.

Scott, D. W. (1979). On optimal and data-based histograms, *Biometrika* **66,** 605–610.

Sekiguchi, H., K. Irikura, and T. Iwata (2000). Fault geometry at the rupture termination of the 1995 Hyogo-ken Nanbu earthquake, *Bull. Seismol. Soc. Am.* **90,** 117–133.

Shi, Z., and S. M. Day (2013). Rupture dynamics and ground motion from 3-D rough-fault simulations, *J. Geophys. Res.* **118,** no. 3, 1122–1141, doi: 10.1002/jgrb.50094.

Shimazaki, H., and S. A. Shinomoto (2007). A method for selecting the bin size of a time histogram, *Neural Comput.* **19,** 1503–1527.

Somerville, P., K. Irikura, R. Graves, S. Sawada, D. Wald, N. Abrahamson, Y. Iwasaki, T. Kagawa, N. Smith, and A. Kowada (1999). Characterizing crustal earthquake slip models for the prediction of strong ground motion, *Seismol. Res. Lett.* **70,** 59–80.

Song, S. G., and L. A. Dalguer (2013). Importance of 1-point statistics in earthquake source modelling for ground motion simulation, *Geophys. J. Int.* **192,** 1255–1270.

Song, S. G., L. A. Dalguer, and P. M. Mai (2013). Pseudo-dynamic source modelling with 1-point and 2-point statistics of earthquake source parameters, *Geophys. J. Int.* **196,** 1770–1786.

Strasser, F. O., M. C. Arango, and J. J. Bommer (2010). Scaling of the source dimensions of interface and intraslab subduction-zone earthquakes with moment magnitude, *Seismol. Res. Lett.* **81,** 941–950.

Stock, S., and E. G. C. Smith (2000). Evidence for different scaling of earthquake source parameters for large earthquakes depending on fault mechanism, *Geophys. J. Int.* **143,** 157–162.

Tinti, E., P. Spudich, and M. Cocco (2005). Earthquake fracture energy inferred from kinematic rupture models on extended faults, *J. Geophys. Res.* **110,** no. B12303, doi: 10.1029/2005JB003644.

Wei, S., R. Graves, D. Helmberger, J. P. Avouac, and J. Jiang (2012). Sources of shaking and flooding during the Tohoku-Oki earthquake: A mixture of rupture styles, *Earth Planet. Sci. Lett.* **333,** 91–100.

Wesnousky, S. G. (1994). The Gutenberg–Richter or characteristic earthquake distribution, which is it? *Bull. Seismol. Soc. Am.* **84,** 1940–1959.

Yen, Y. T., and H. F. Ma (2011). Source-scaling relationship for M 4.6–8.9 earthquakes, specifically for earthquakes in the collision zone of Taiwan, *Bull. Seismol. Soc. Am.* **101,** 464–481.

Zhang, L., P. M. Mai, K. K. S. Thingbaijam, H. N. Razafindrakoto, and M. G. Genton (2015). Analysing earthquake slip models with the spatial prediction comparison test, *Geophys. J. Int.* **200,** 185–198.

Zielke, O., and P. M. Mai (2016). Sub-patch roughness in earthquake rupture investigations, *Geophys. Res. Lett.* **43,** no. 5, 1893–1900, doi: 10.1002/2015GL067084.

Division of Physical Science and Engineering
King Abdullah University of Science and Technology
3109, Building 1
Thuwal 23955-6900
Kingdom of Saudi Arabia
k.thingbaijam@kaust.edu.sa
martin.mai@kaust.edu.sa

Manuscript received 25 October 2015;
Published Online 12 July 2016;
Corrected Online 13 April 2016